Monthly Notices
of the
ROYAL ASTRONOMICAL SOCIETY

MNRAS **479,** 2007–2015 (2018)
Advance Access publication 2018 June 6

doi:10.1093/mnras/sty1478

Hydrogen transfer reactions of interstellar complex organic molecules

S. Álvarez-Barcia, P. Russ, J. Kästner and T. Lamberts★†

Institute for Theoretical Chemistry, University of Stuttgart, Pfaffenwaldring 55, D-70569 Stuttgart, Germany

Accepted 2018 May 25. Received 2018 May 24; in original form 2018 April 9

ABSTRACT

Radical recombination has been proposed to lead to the formation of complex organic molecules (COMs) in ices rich in carbon monoxide (CO) in the early stages of star formation. These COMs can then undergo hydrogen addition and abstraction reactions leading to a higher or lower degree of saturation. Here, we have studied 14 hydrogen transfer reactions for the molecules glyoxal, glycoaldehyde, ethylene glycol, and methylformate, and an additional three reactions where CH_nO fragments are involved. Over-the-barrier reactions are possible only if tunneling is invoked in the description at low temperature. Therefore, the rate constants for the studied reactions are calculated using instanton theory that takes quantum effects into account inherently. The reactions were characterized in the gas phase, but this is expected to yield meaningful results for CO-rich ices due to the minimal alteration of reaction landscapes by the CO molecules. We found that rate constants should not be extrapolated based on the height of the barrier alone, since the shape of the barrier plays an increasingly larger role at decreasing temperature. It is neither possible to predict rate constants based only on considering the type of reaction, the specific reactants and functional groups play a crucial role. Within a single molecule, though, hydrogen abstraction from an aldehyde group seems to be always faster than hydrogen addition to the same carbon atom. Reactions that involve heavy-atom tunneling, e.g. breaking or forming a C–C or C–O bond, have rate constants that are much lower than those where H transfer is involved.

Key words: astrochemistry – methods: laboratory – ISM: molecules.

1 INTRODUCTION

Thanks to the unprecedented sensitivity of the Atacama Large Millimeter Array the detection and quantification of interstellar complex organic molecules (COMs) have become more and more within reach. A COM in the context of astrochemistry is loosely defined as a molecule consisting of more than six H, C, O, and/or N atoms. Typical gas-phase abundances of such molecules are only of the order of $<10^{-8}$ with respect to H_2 (Jørgensen et al. 2012; Halfen, Ilyushin & Ziurys 2015; Taquet et al. 2015; López-Sepulcre et al. 2017) with even lower abundances for deuterated species (Belloche et al. 2016). These molecules are currently thought to find their origins in the CO-rich top layers of the grain ice mantle (Boogert, Gerakines & Whittet 2015) where the H + CO reaction network has been shown to lead to the formation of the parent species formaldehyde (FA), H_2CO, and methanol (ME), CH_3OH (Tielens & Hagen 1982; Hiraoka et al. 1998; Watanabe & Kouchi 2002; Fuchs et al. 2009). Furthermore, besides hydrogen addition reactions, also hydrogen abstraction reactions can take place that decrease the number of H atoms on the carbon monoxide (CO) backbone (Nagaoka, Watanabe & Kouchi 2005; Nagaoka, Watanabe & Kouchi 2007). Although it has been suggested that formaldehyde and methanol may desorb from the grain surface and subsequently react in the gas phase to yield more complex species (Bottinelli et al. 2004; Balucani, Ceccarelli & Taquet 2015; Taquet et al. 2017), a variety of COMs have been detected in cold interstellar regions (Öberg et al. 2010; Bacmann et al. 2012; Vastel et al. 2014). This indicates that low-temperature surface chemistry can play an important role in the formation of larger species.

In fact the H + CO reaction network has evolved into a network where carbon–carbon bonds can be formed via radical–radical reactions between the 'fundamental' radicals that are created as intermediates, i.e. HCO, CH_2OH, and CH_3O. Most of these reactions have been studied experimentally in various ways (Butscher et al. 2015; Fedoseev et al. 2015; Chuang et al. 2016; Butscher et al. 2017; Chuang et al. 2017; Fedoseev et al. 2017) and they have also been proposed by and are included in a number of astrochemical model studies (Garrod, Widicus Weaver & Herbst 2008; Woods et al. 2012; Coutens et al. 2018). Similar conclusions are also supported by observational work for specific species (Li et al. 2017; Rivilla et al. 2017). Despite this significant amount of investigations, relatively little is known about the reaction rate constants at

★ E-mail: a.l.m.lamberts@lic.leidenuniv.nl
† Present address: Leiden Institute of Chemistry, Gorlaeus Laboratories, Leiden University, PO Box 9502, NL-2300 RA Leiden, the Netherlands.

low temperature, while these are the crucial parameters needed to constrain modelling studies.

Here, we focus on hydrogen addition and abstraction reactions of species with two carbon atoms and two oxygen atoms, i.e. methylformate (MF), glyoxal (GX), glycoaldehyde (GA), and ethylene glycol (EG) (Section 3.1). Several other reactions are discussed as well where a C–C or C–O bond is formed via an over-the-barrier reaction between a CH_nO radical and FA (Section 3.2). Finally, we provide an overview of reaction rate constants previously calculated for the CO + H network involving both formaldehyde and methanol (Andersson, Goumans & Arnaldsson 2011; Goumans 2011b; Goumans & Kästner 2011; Song & Kästner 2017) (Section 3.3). Low-temperature reaction rate constants have been calculated for the first time using instanton theory and serve as an order of magnitude estimate implementation in astrochemical models. We will also comment on the possibility to generalize rate constants based only on the type of reaction.

2 COMPUTATIONAL DETAILS

Two different levels of theory have been used throughout this study in order to balance the computational cost and chemical accuracy. All calculated activation and reaction energies, as well as the rate constants, have been calculated with density functional theory (DFT). In particular, the functional MPWB1K combined with the basis set def2-TZVP has been used. The accuracy of the activation energies or barrier heights is ensured by benchmarking these values to a better level of theory, namely CCSD(T)-F12/VTZ-F12.

Optimizations of the stationary points and corresponding energies were computed at the MPWB1K/def2-TZVP level (Zhao & Truhlar 2004; Weigend & Ahlrichs 2005; Weigend 2006). Geometry optimizations (minima and transition states) were done with DL-FIND (Kästner et al. 2009) in ChemShell (Sherwood et al. 2003; Metz et al. 2014). For the electronic structure computations (energies, gradients, and Hessians) Gaussian 09 (Frisch et al. 2009) has been employed. Self-consistent field (SCF) cycles were stopped when the convergence, as defined in G09, reached 1×10^{-9} Hartree. A pruned (99 590) grid (ultrafine grid) was employed, having 99 radial shells and 590 angular points per shell.

The MPWB1K functional has been previously benchmarked in order to predict the correct bond dissociation energy of methyl formate, for which accurate results were obtained (Li et al. 2016). Furthermore, MPWB1K was developed to take into account weak interactions such as those found in the pre-reactive complexes (PRCs) treated here. In order to confirm the use of this functional for the current study, single-point energy calculations at the RHF-UCCSD(T)-F12/VTZ-F12//MPWB1K/def2-TZVP level (Knowles, Hampel & Werner 1993, 2000; Deegan & Knowles 1994; Adler, Knizia & Werner 2007; Peterson, Adler & Werner 2008; Knizia, Adler & Werner 2009) were carried out and are discussed in Appendix A.

The instanton method based on Feynman path integral theory using the semiclassical approximation was used to compute the reaction rate constants (Langer 1967, 1969; Miller 1975; Callan & Coleman 1977; Coleman 1977; Gildener & Patrascioiu 1977; Affleck 1981; Coleman 1988; Hänggi, Talkner & Borkovec 1990; Benderskii, Makarov & Wight 1994; Messina, Schenter & Garrett 1995; Richardson & Althorpe 2009; Kryvohuz 2011; Althorpe 2011; Rommel, Goumans & Kästner 2011; Rommel & Kästner 2011; Kryvohuz 2014; Richardson 2016). For a given temperature, it provides the most probable tunnelling path, the instanton, which connects the reactant and product valleys of the potential energy surface. Instanton theory is applicable whenever the temperature is low enough for the instanton to spread out. At higher temperatures, the instanton collapses to a point that renders the theory inapplicable. For most barriershapes this collapse happens at the crossover temperature (T_c) (Gillan 1987; Álvarez-Barcia, Flores & Kästner 2014),

$$T_c = \frac{\hbar\,\Omega}{2\pi k_B}, \tag{1}$$

with Ω being the absolute value of the imaginary frequency corresponding to the transition mode and k_B corresponding to Boltzmann's constant. T_c qualitatively indicates at which temperature the reaction is dominated by tunnelling ($T < T_c$) or by the thermal activation ($T > T_c$).

Instanton paths were optimized via a quasi Newton–Raphson method (Rommel et al. 2011; Rommel & Kästner 2011). Energies, gradients, and Hessians were provided by Gaussian 09, but instanton optimizations are done in DL-FIND. The instanton path was discretised using 80 images, except for reactions MF3 and MF4 where 158 images were employed at $T \leq 100$ K and 314 images for MF4 at 75 K.

This study focuses on unimolecular rate constants, i.e. on the Langmuir–Hinshelwood mechanism. Both reactants are adsorbed on the surface, approach each other via diffusion and form a PRC on the surface. This PRC can then decay to yield the reaction products via a unimolecular process. It has been shown in the recent literature that often gas-phase calculations of stationary points offer a reasonably accurate approach for representing the very same reactions on an ice surface. This even holds for ices composed of water molecules as typical changes of the activation energy are roughly only 1–2 kJ mol^{-1} (Rimola et al. 2014; Song & Kästner 2017; Lamberts 2018). However, in particular cases, larger energy differences may be found (Lamberts & Kästner 2017b) and to which extent surface molecules may affect the binding orientation is currently unclear. Finally, adsorption on a surface is simulated by keeping the rotational partition function constant between the reactant and transition state. For more information regarding this approach the reader is referred to Meisner, Lamberts & Kästner (2017) and Lamberts & Kästner (2017a).

3 RESULTS

We simulated a total of 14 reactions revolving around the molecules glyoxal (GX), glycoaldehyde (GA), ethylene glycol (EG), and methylformate (MF), an additional three reactions where reactions of CH_nO fragments with H_2CO are involved (FAR), and discuss the results in the light of the six previously studied reactions with carbon monoxide (CO), formaldehyde (FA), and methanol (ME). To structure the analysis, the reactions are labelled according to their type, except for the FARn series:

(1) H addition to aldehyde carbon – MF, GX, GA, CO, FA
(2) H addition to aldehyde oxygen – MF, GX, GA, FA
(3) H abstraction from aldehyde carbon – MF, GX, GA, FA
(4) H abstraction from methyl group – MF, EG, ME
(5) H addition to etheric oxygen – MF
(6) H abstraction from alcohol oxygen – GA, EG, ME

Note that we expect all reactions studied and discussed here to take place in an environment where CO is the main component of the ice mantle. Due to the general weak interactions of this molecule, we expect that the activation energies calculated here in the gas phase will be similar to those in the presence of a CO environment. For instance for the reactions H + CO and H + H_2CO this has been

Table 1. Activation energies with respect to the pre-reactive complexes computed at the MPWB1K/def2-TZVP level with ($\Delta E^{0,\ddagger}$) and without ($\Delta E^{\ddagger}$) Zero point energy (ZPE) correction. T_c and rate constants (k at 75 K unless indicated otherwise) are also included.

	$\Delta E^{\ddagger}$ (kJ mol^{-1})	$\Delta E^{0,\ddagger}$ (kJ mol^{-1})	T_c (K)	k (75 K) s^{-1}
H + MF				
MF1	38.1	41.2	262.2	3.6×10^{-1}
MF2	59.0	59.9	400.4	1.7
MF3	46.6	38.1	365.8	3.4[a]
MF4	51.2	42.8	345.1	1.1×10^{-1}
MF5	146.0	149.9	496.7	3.8×10^{-33}
H + GX				
GX1	15.1	15.1	179.9	9.6×10^{6}
GX2	29.8	31.7	298.9	1.8×10^{3}
H + GA				
GA1	19.0	20.8	203.4	2.8×10^{5}
GA2	38.5	39.8	342.5	2.8×10^{2}
GA3	24.3	14.6	317.6	6.8×10^{7}
GA4	27.3	20.6	333.5	2.6×10^{4}
GA6	55.8	46.2	405.2	9.6×10^{-1}
H + EG				
EG4	28.4	19.3	303.3	3.5×10^{6}
EG6	54.1	42.2	406.3	2.1×10^{3}[b]
FARn				
FAR1	30.6	22.2	336.6	2.0×10^{3}[c]
FAR2	44.8	48.5	151.9	4.6×10^{-9}[d]
FAR3	19.9	24.5	58.3	3.9×10^{-11}[c]

[a] At 80 K.
[b] At 90 K.
[c] At 50 K.
[d] At 65 K.

confirmed by Rimola et al. (2014). Therefore, the values presented here are thought to be a good representation of the situation in the interstellar medium.

3.1 Reactions with MF, GX, GA, and EG

Activation energies for the reactions described in this section and in Section 3.2 can be found in Table 1. T_c as an indication of the importance of tunneling, and the calculated low-temperature rate constants are presented as well. A schematic representation of the reactions with methyl formate, glyoxal, glycoaldehyde, and ethylene glycol is given in Fig. 1. The temperature-dependence of the calculated rate constants is depicted in Figs 2–6. The reaction of the hydrogen atom with methyl formate has been studied in order to determine if it is an efficient destruction channel. The addition and abstraction reactions of H with glyoxal, glycoaldehyde, and ethylene glycol serve to study the sequential hydrogenation steps. In this way the same reaction type (see above) can be compared between various molecules, and it can be determined whether or not addition is faster than abstraction. Note that the reaction abstracting a hydrogen atom from glyoxal (GX3) could not be studied, because according to the benchmark study the most accurate value for the activation energy cannot be validated: the difference between the DFT and CCSD(T)-F12 value is too large and moreover multireference effects prevent the CCSD(T)-F12 value from being trusted.

Reactions with MF

$$H + MF \longrightarrow CH_3OCOH_2 \quad (MF1)$$

$$H + MF \longrightarrow CH_3OCHOH \quad (MF2)$$

$$H + MF \longrightarrow CH_3OCO + H_2 \quad (MF3)$$

$$H + MF \longrightarrow CH_2OCOH + H_2 \quad (MF4)$$

$$H + MF \longrightarrow HCO + CH_3OH \quad (MF5)$$

Reactions with GX

$$H + GX \longrightarrow (H_2CO)CHO \quad (GX1)$$

$$H + GX \longrightarrow (HCOH)CHO \quad (GX2)$$

$$H + GX \longrightarrow (CO)CHO + H_2 \quad (GX3)$$

Reactions with GA

$$H + GA \longrightarrow (H_2CO)CH_2OH \quad (GA1)$$

$$H + GA \longrightarrow (HCOH)CH_2OH \quad (GA2)$$

$$H + GA \longrightarrow (CO)CH_2OH + H_2 \quad (GA3)$$

$$H + GA \longrightarrow (HCO)CHOH + H_2 \quad (GA4)$$

$$H + GA \longrightarrow (HCO)CH_2O + H_2 \quad (GA6)$$

Reactions with EG

$$H + EG \longrightarrow (HOCH)CH_2OH + H_2 \quad (EG4)$$

$$H + EG \longrightarrow (OCH_2)CH_2OH + H_2 \quad (EG6)$$

3.2 Reactions between FA and CH_nO

Although the COMs discussed above have been proposed to be formed mainly through radical–radical reactions, reactions between a neutral and radical species may also lead to the formation of a C–C or C–O bond. The reactions between H_2CO and CH_3O or HCO (Butscher et al. 2017) are therefore studied as well in order to compare their efficiency to other radical-neutral reactions as well as to fast barrierless radical–radical reactions.

Reactions FAR1 and FAR2 are in direct competition with each other, see also Fig. 7.

$$H_2CO + CH_3O \longrightarrow CH_3OH + HCO \quad (FAR1)$$

$$H_2CO + CH_3O \longrightarrow CH_3OCH_2O \quad (FAR2)$$

$$H_2CO + HCO \longrightarrow (HCO)CH_2O \quad (FAR3)$$

3.3 Reactions with CO, FA, and ME

Prior to discussing hydrogen transfer reactions in COMs, this section summarizes previous theoretical studies related to the H + CO reaction network for cases where calculations have also been performed with instanton theory. The main results in terms of activation energy and reaction rate constant from those studies are listed in Table 2.

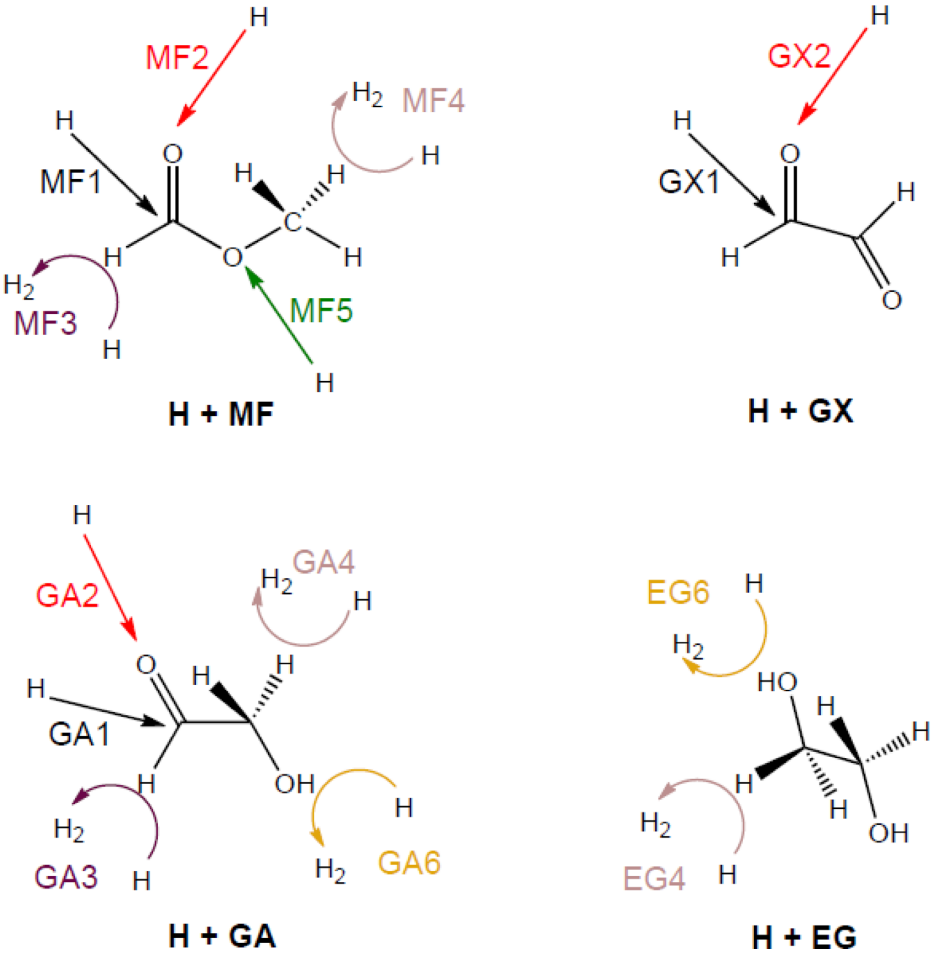

Figure 1. Schematic representation of the reactions shown in Section 3.1. MF, GX, GA, and EG correspond to methylformate, glyoxal, glycoaldehyde, and ethylene glycol, respectively.

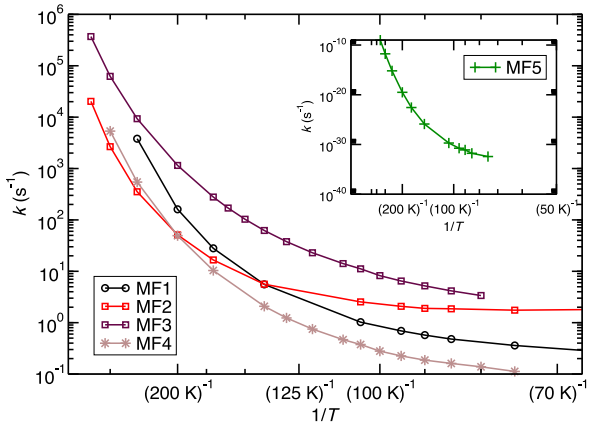

Figure 2. Unimolecular rate constants (in s^{-1}) calculated with instanton theory for the MF + H reactions.

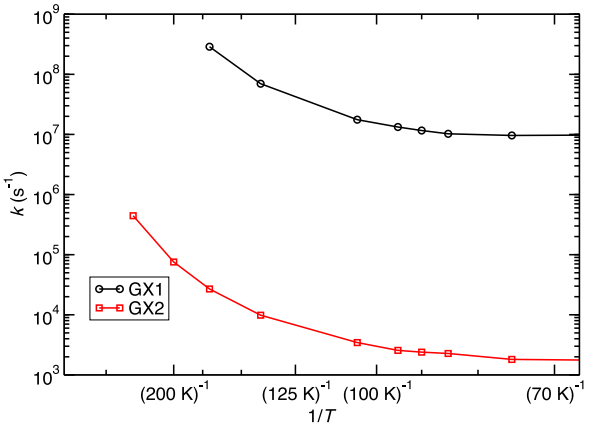

Figure 3. Unimolecular rate constants (in s^{-1}) calculated with instanton theory for the GX + H reactions.

Reaction with CO

Unimolecular rate constants for the H + CO system have been theoretically calculated by Andersson et al. (2011), using a PES previously obtained by Keller et al. (1996):

$$H + CO \longrightarrow HCO \qquad (CO1)$$

Reactions with FA

The reaction of H and H_2CO (H + FA) has been theoretically studied by both Goumans (2011a) and Song & Kästner (2017).

$$H + FA \longrightarrow CH_3O \qquad (FA1)$$

$$H + FA \longrightarrow CH_2OH \qquad (FA2)$$

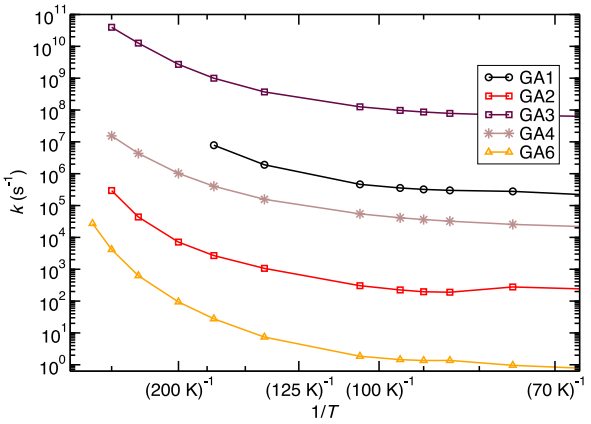

Figure 4. Unimolecular rate constants (in s^{-1}) calculated with instanton theory for the GA + H reactions.

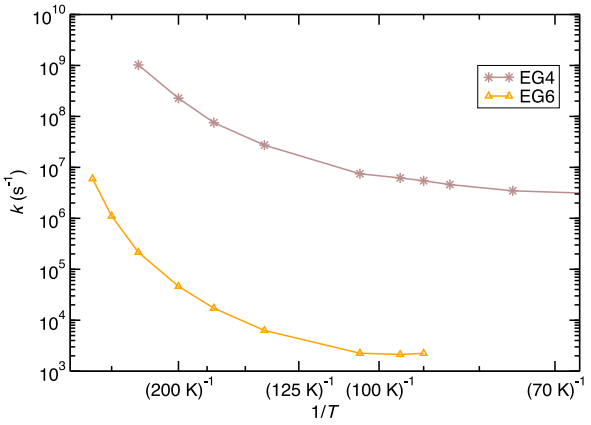

Figure 5. Unimolecular rate constants (in s^{-1}) calculated with instanton theory for the EG + H reactions.

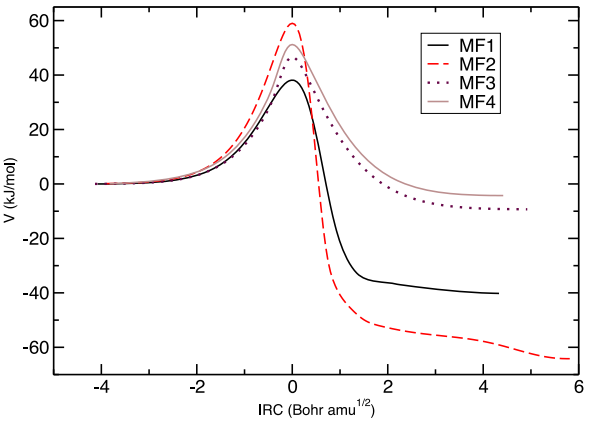

Figure 6. Intrinsic reaction coordinates for reactions MF1–MF4.

$$H + FA \longrightarrow H_2 + HCO \qquad (FA3)$$

Reactions with ME

The abstraction of H from methanol has been studied theoretically by Goumans & Kästner (2011).

$$H + ME \longrightarrow CH_2OH + H_2 \qquad (ME4)$$

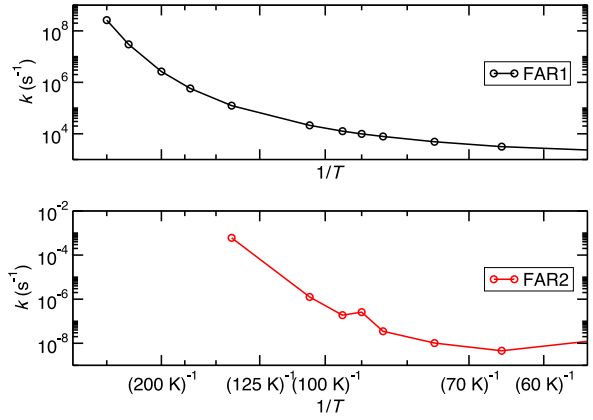

Figure 7. Unimolecular rate constants (in s^{-1}) calculated with instanton theory for the reactions of FA with CH_nO fragments (FARn).

Table 2. Activation energies including ZPE ($\Delta E^{0,\ddagger}$) and unimolecular rate constants (k) obtained from literature values.

	$\Delta E^{0,\ddagger}$ (kJ mol^{-1})	k s^{-1}
H + CO		
CO1	12.4 + ∼1.2[a]	2.1×10^5 at 5 K [1]
H + FA		
FA1	15.8–17.9	1.5×10^5–2.0×10^6 at 70 K [2]
FA2	43.3–47.1	4.0×10^1–9.0×10^1 at 75 K [2]
FA3	20.5–25.2	4.0×10^5–1.0×10^6 at 70 K [2]
H + ME		
ME4	30.2	– [3]
ME6	46.4	– [3]

Notes. [1] Andersson, Goumans & Arnaldsson (2011); [2] Song & Kästner (2017); [3] Goumans & Kästner (2011). [a] ZPE calculated in this work (CCSD(T)-F12/VTZ-F12)

$$H + ME \longrightarrow CH_3O + H_2 \qquad (ME6)$$

4 DISCUSSION

4.1 Hydrogen addition and abstraction reactions

For most of the reactions, the rate constants level off at a given temperature, especially below 80 K.

The reactions of the hydrogen atom with methylformate overall have the highest activation energies, indicating that MF is quite stable with respect to attack by a H radical. Reaction MF5 is a special case, where a C–O bond is being broken, while an O–H bond is formed, which is most likely the reason for the corresponding activation energy, or high barrier.

Comparing between the various reaction types, Figs 2 and 4 show that the H abstractions from the H of the HC=O group (type 3) occur with high reaction rate constants. The H abstraction from the –OH group (type 6), on the other hand, appears to be very unfavourable with barriers larger than ∼50 kJ mol^{-1} (Figs 4 and 5). This is consistent with previous results obtained for the reaction between hydrogen and methanol. The barrier between reactions ME4 and ME6 differs by 16 kJ mol^{-1}, in line with the experimental work of Chuang et al. (2016) and Nagaoka et al. (2007).

Generalizing reaction types 1, 2, and 4 is not trivial. The activation energies for type 1 are always lower than those for type 2, when compared within the same molecule (FA, MF, GX, and GA). For

instance the formation of CH_3O is preferred over the formation of CH_2OH, contrary to the findings of Butscher et al. (2015), but in line with those of Chuang et al. (2016). The rate constants for type 1 are indeed higher than those for type 2 for reactions with FA, GX, and GA, but MF is a special case. Similarly for type 4, where the activation energies are higher than for type 2 and consequently the rate constants are lower for GA, but again reaction MF2 deviates. At temperatures below 200 K the reaction rate constant for MF2 crosses first that of MF4 and later that of MF1 even though the barrier is higher. The origin of this behaviour lies in the barrier width. Tunneling namely depends both on the barrier height and width as well as on the effective mass of the system. The narrower the barrier at low-energy incidence, the more tunneling may be expected. This can be visualized with the help of intrinsic reaction coordinates (IRCs). The IRC curves are calculated using the algorithm described by Meisner et al. (2017) and Hratchian & Schlegel (2004). They are presented in Fig. 6, note that these do not include ZPE corrections and therefore relate to the barrier height $\Delta E^{\ddagger}$ of Table 1.

Finally, it cannot be said that in general addition is more efficient than abstraction or vice versa, e.g. compare reaction types 1 and 2 against 3, 4, and 6.

4.2 Reactions between FA and CH_nO

At decreasing temperatures tunneling dominates a reaction more and more. This can explain the large difference between the low-temperature value for the rate constant of reaction FAR2 compared to FAR1. For FAR2 a C–O bond is formed and as heavy-atom tunneling is less efficient than hydrogen atom tunneling, the rate constant is much lower than what would be expected from the barrier height only (compare for instance MF4, GA6, and FAR2). Similarly for the reaction of FA with HCO, where a C–C bond is formed (FAR3), again the low-temperature rate constant is very low. Note also the lower values for the T_c of FAR2 and FAR3 compared to the hydrogen transfer reactions, indicating that tunneling also sets in at lower temperatures. Comparing the rate constant to the typical value assumed for radical–radical barrierless reactions, $\sim 10^{12}$ s^{-1}, it is clear that these reactions are much less likely to contribute to COM formation. On that note we do wish to stress, however, to keep in mind that although radical–radical reactions may be able to proceed without a barrier, this does not mean that all reaction pathways are open, see for instance Lamberts (2018).

5 ASTROCHEMICALLY RELEVANT CONCLUSIONS

Unimolecular reaction rate constants have been calculated and are provided for hydrogen addition and abstraction reactions from methylformate, glyoxal, glycoaldehyde, an ethylene glycol and are thus available to be implemented in both rate-equation and kinetic Monte Carlo models aimed at studying the formation of COMs at low temperatures.

Our results are generally in agreement with experimental work, although some discrepancies exist on the efficiency of specific reaction paths, such as the formation of CH_2OH or CH_3O after hydrogen abstraction from methanol, which impacts on the ease of methylformate formation (for which CH_3O is needed) or ethylene glycol formation (for which CH_2OH is required). A microscopic model aiming to reproduce experiments may be able to provide a clear picture of how the reactions are intertwined with each other.

The reaction $H + GX- < (CO)CHO + H_2$ could not be studied and thus deserves further attention.

We found that one cannot predict average rate constants solely based on the type of the reaction. The spread in the low-temperature rate constant can be roughly seven orders of magnitude for a single reaction type (e.g. hydrogen addition to an aldehyde carbon) showing a strong dependence on the other functional groups that are attached to the carbon backbone.

Within a single molecule, on the other hand, one can loosely say that hydrogen abstraction from an aldehyde group is faster than hydrogen addition to the same carbon. Both of these have a rate constant that is larger than hydrogen abstraction from a methyl group.

Care should be taken with extrapolating rate constants based on the height of the barrier alone, as calculations show that reactions with narrow barriers can have rate constants at low temperature that are higher than those with a lower activation energy.

Reactions that include the breakage or formation of a bond between two heavy atoms generally have low-temperature rate constants that are much lower than those for hydrogen addition or abstraction reactions as a result of the low efficiency of tunneling when heavy atoms are involved.

ACKNOWLEDGEMENTS

The authors acknowledge support for computer time by the state of Baden-Württemberg through bwHPC and the Germany Research Foundation (DFG) through grant nos. INST 40/467-1FUGG and SFB 716/C.6. This project was financially supported by the European Union's Horizon 2020 research and innovation programme (grant agreement no. 646717, TUNNELCHEM), the Alexander von Humboldt Foundation, the Netherlands Organisation for Scientific Research (NWO) via a VENI fellowship (722.017.008), and the COST Action CM1401 via an STSM travel grant.

REFERENCES

Adler T. B., Knizia G., Werner H.-J., 2007, J. Chem. Phys., 127, 221106
Affleck I., 1981, Phys. Rev. Lett., 46, 388
Althorpe S. C., 2011, J. Chem. Phys., 134, 114104
Andersson S., Goumans T., Arnaldsson A., 2011, Chem. Phys. Lett., 513, 31
Álvarez-Barcia S., Flores J. R., Kästner J., 2014, J. Phys. Chem. A, 118, 78
Bacmann A., Taquet V., Faure A., Kahane C., Ceccarelli C., 2012, A&A, 541, L12
Balucani N., Ceccarelli C., Taquet V., 2015, MNRAS, 449, L16
Belloche A., Müller H. S. P., Garrod R. T., Menten K. M., 2016, A&A, 587, A91
Benderskii V. A., Makarov D. E., Wight C. A., 1994, Adv. Chem. Phys., 88, 55
Boogert A. A., Gerakines P. A., Whittet D. C., 2015, ARA&A, 53, 541
Bottinelli S. et al., 2004, ApJ, 615, 354
Butscher T., Duvernay F., Theule P., Danger G., Carissan Y., Hagebaum-Reignier D., Chiavassa T., 2015, MNRAS, 453, 1587
Butscher T., Duvernay F., Rimola A., Segado-Centellas M., Chiavassa T., 2017, Phys. Chem. Chem. Phys., 19, 2857
Callan C. G. Jr, Coleman S., 1977, Phys. Rev. D, 16, 1762
Chuang K.-J., Fedoseev G., Ioppolo S., van Dishoeck E. F., Linnartz H., 2016, MNRAS, 455, 1702
Chuang K.-J., Fedoseev G., Qasim D., Ioppolo S., van Dishoeck E. F., Linnartz H., 2017, MNRAS, 467, 2552
Coleman S., 1977, Phys. Rev. D, 15, 2929
Coleman S., 1988, Nucl. Phys. B, 298, 178
Coutens A., Viti S., Rawlings J. M. C., Beltrán M. T., Holdship J., Jiménez-Serra I., Quénard D., Rivilla V. M., 2018, MNRAS, 475, 2016
Deegan M. J. O., Knowles P. J., 1994, Chem. Phys. Lett., 227, 321

Fedoseev G., Cuppen H. M., Ioppolo S., Lamberts T., Linnartz H., 2015, MNRAS, 448, 1288
Fedoseev G., Chuang K.-J., Ioppolo S., Qasim D., van Dishoeck E. F., Linnartz H., 2017, ApJ, 842, 52
Frisch M. J. et al., 2009, Gaussian 09 Revision D.01, Wallingford CT
Fuchs G. W., Cuppen H. M., Ioppolo S., Romanzin C., Bisschop S. E., Andersson S., van Dishoeck E. F., Linnartz H., 2009, A&A, 505, 629
Garrod R. T., Widicus Weaver S. L., Herbst E., 2008, ApJ, 682, 283
Gildener E., Patrascioiu A., 1977, Phys. Rev. D, 16, 423
Gillan M. J., 1987, J. Phys. C, 20, 3621
Goumans T. P. M., 2011a, MNRAS, 413, 26150
Goumans T. P. M., 2011b, MNRAS, 415, 3129
Goumans T. P. M., Kästner J., 2011, J. Phys. Chem. A, 115, 10767
Halfen D. T., Ilyushin V. V., Ziurys L. M., 2015, ApJ, 812, L5
Hänggi P., Talkner P., Borkovec M., 1990, Rev. Mod. Phys., 62, 251
Hiraoka K., Miyagoshi T., Takayama T., Yamamoto K., Kihara Y., 1998, ApJ, 498, 710
Hratchian H. P., Schlegel H. B., 2004, J. Chem. Phys., 120, 9918
Jørgensen J. K., Favre C., Bisschop S. E., Bourke T. L., van Dishoeck E. F., Schmalzl M., 2012, ApJ, 757, L4
Kästner J., Carr J. M., Keal T. W., Thiel W., Wander A., Sherwood P., 2009, J. Phys. Chem. A, 113, 11856
Keller H., Floethmann H., Dobbyn A. J., Schinke R., Werner H., Bauer C., Rosmus P., 1996, J. Chem. Phys., 105, 4983
Knizia G., Adler T. B., Werner H.-J., 2009, J. Chem. Phys., 130, 054104
Knowles P. J., Hampel C., Werner H.-J., 1993, J. Chem. Phys., 99, 5219
Knowles P. J., Hampel C., Werner H.-J., 2000, J. Chem. Phys., 112, 3106
Kryvohuz M., 2011, J. Chem. Phys., 134, 114103
Kryvohuz M., 2014, J. Phys. Chem. A, 118, 535
Lamberts T., 2018, Astron. Astrophys. Lett., preprint (arXiv:1806.02990)
Lamberts T., Kästner J., 2017a, J. Phys. Chem. A, 121, 9736
Lamberts T., Kästner J., 2017b, ApJ, 846, 43
Langer J. S., 1967, Ann. Phys. (N.Y.), 41, 108
Langer J. S., 1969, Ann. Phys. (N.Y.), 54, 258
Lee T. J., 2003, Chem. Phys. Lett., 372, 362
Li X., Xu X., You X., Truhlar D. G., 2016, J. Phys. Chem. A, 120, 4025
Li J. et al., 2017, ApJ, 849, 115
López-Sepulcre A. et al., 2017, A&A, 606, A121
Meisner J., Lamberts T., Kästner J., 2017, ACS Earth Space Chem., 1, 399
Meisner J., Markmeyer M. N., Bohner M. U., Kastner J., 2017, Phys. Chem. Chem. Phys., 19, 23085
Messina M., Schenter G. K., Garrett B. C., 1995, J. Chem. Phys., 103, 3430
Metz S., Kästner J., Sokol A. A., Keal T. W., Sherwood P., 2014, WIREs Comput. Mol. Sci., 4, 101
Miller W. H., 1975, J. Chem. Phys., 62, 1899
Nagaoka A., Watanabe N., Kouchi A., 2005, ApJ, 624, L29
Nagaoka A., Watanabe N., Kouchi A., 2007, J. Phys. Chem. A, 111, 3016
Öberg K. I., Bottinelli S., Jørgensen J. K., van Dishoeck E. F., 2010, ApJ, 716, 825
Peterson K. A., Adler T. B., Werner H.-J., 2008, J. Chem. Phys., 128, 084102
Richardson J. O., 2016, J. Chem. Phys., 144, 114106
Richardson J. O., Althorpe S. C., 2009, J. Chem. Phys., 131, 214106
Rimola A., Taquet V., Ugliengo P., Balucani N., Ceccarelli C., 2014, A&A, 572, A70
Rivilla V. M., Beltrán M. T., Cesaroni R., Fontani F., Codella C., Zhang Q., 2017, A&A, 598, A59
Rommel J. B., Kästner J., 2011, J. Chem. Phys., 134, 184107
Rommel J. B., Goumans T. P. M., Kästner J., 2011, J. Chem. Theory Comput., 7, 690
Sherwood P. et al., 2003, J. Mol. Struct. (THEOCHEM), 632, 1
Shiozaki T., Werner H.-J., 2011, J. Chem. Phys., 134, 184104
Shiozaki T., Knizia G., Werner H.-J., 2011, J. Chem. Phys., 134, 034113
Song L., Kästner J., 2017, ApJ, 850, 118
Taquet V., López-Sepulcre A., Ceccarelli C., Neri R., Kahane C., Charnley S. B., 2015, ApJ, 804, 81
Taquet V., Wirström E. S., Charnley S. B., Faure A., López-Sepulcre A., Persson C. M., 2017, A&A, 607, A20
Tielens A. G. G. M., Hagen W., 1982, A&A, 114, 245
Vastel C., Ceccarelli C., Lefloch B., Bachiller R., 2014, ApJ, 795, L2
Watanabe N., Kouchi A., 2002, ApJ, 571, L173
Weigend F., 2006, Phys. Chem. Chem. Phys., 8, 1057
Weigend F., Ahlrichs R., 2005, Phys. Chem. Chem. Phys., 7, 3297
Woods P. M., Kelly G., Viti S., Slater B., Brown W. A., Puletti F., Burke D. J., Raza Z., 2012, ApJ, 750, 19
Zhao Y., Truhlar D. G., 2004, J. Phys. Chem. A, 108, 6908

APPENDIX A: BENCHMARK CALCULATIONS

RHF-UCCSD(T)-F12/VTZ-F12//MPWB1K/def2-TZVP single-point energy calculations were performed in order to check if MPWB1K provides a suitable description of the energy landscape for the reactions studied here. In general, the CCSD(T)-F12 method can be seen as the gold standard for obtaining relative energies for systems that are well-described by a single reference wavefunction. This is typically assumed to be the case when the so-called T_1 and D_1 diagnostics are smaller than the commonly used threshold values ($T_1 \leq 0.02$ and $D_1 \leq 0.05$) (Lee 2003). Here, this is the case for reactions MF2, MF4, GX1, GA1, GA4, and EG4. These reactions are included in Table A1 and the deviation in the activation energy ranges between 0.4 and 3.3 kJ mol^{-1}, i.e. within chemical accuracy.

Furthermore, the extent of the multireference character for reaction type 2 (MF2, GX2, and GA2) was tested via MRCI-F12/VTZ-F12//MPWB1K/def2-TZVP calculations (Peterson et al. 2008; Shiozaki, Knizia & Werner 2011; Shiozaki & Werner 2011) for a reaction of the same type, but with a smaller reactant: $H + H_2CO- < CH_2OH$. These single-point energy calculations indicate that the reaction does not have a large multireference character. First, the configuration interaction (CI) coefficients for the reference wavefuntion of the transition state structure correspond to 0.934, −0.124, 0.074, and −0.051. In addition, the activation energies at DFT, CCSD(T)-F12, and MRCI-F12 level are similar (38.8, 40.6, and 36.4 kJ mol^{-1}, respectively). Therefore, here the CCSD(T)-F12 method is considered to be a reasonable reference method for these specific three reactions as well, i.e. for a H addition to an aldehyde oxygen.

The MPWB1K functional has been shown to provide a good description for 9 out of the 17 reactions dealt with here, with reaction types 1 to 4 being included in this benchmark. There-

Table A1. Activation energies without zero-point energy correction ($\Delta E^{\ddagger}$) with respect to the separated reactants (in kJ mol^{-1}) computed at the MPWB1K/def2-TZVP level (DFT) and RHF-UCCSD(T)-F12/VTZ-F12//MPWB1K/def2-TZVP (CC).

	$\Delta E^{\ddagger}$ DFT	$\Delta E^{\ddagger}$ CC
MF2	58.8	59.2
MF3	46.5	*48*[a]
MF4	51.1	52.8
GX1	14.7	15.4
GX2	29.7	*31*[a]
GA1	18.5	17.5
GA2	38.2	*37*[a]
GA4	26.5	29.5
EG4	27.9	31.2

[a] Single-reference character confirmed, see the text.

Table A2. Activation energies without zero-point energy correction ($\Delta E^{\ddagger}$) with respect to the separated reactants (in kJ mol^{-1}) computed with several functionals and the def2-TZVP basis set.

	MPWB1K	M06-2X	MPW1B95	MN12-SX	N12-SX	SOGGA11-X
H + MF						
MF1	38.0	39.2	35.0	33.7	43.1	39.1
MF2	58.8	57.1	52.0	56.7	59.3	61.3
MF3	46.5	50.5	38.0	43.3	43.5	46.2
MF4	51.1	55.1	44.3	50.1	48.7	52.5
MF5	145.8	138.0	131.5	142.3	137.6	148.1
H + GX						
GX1	14.7	17.0	12.9	8.3	21.9	15.7
GX2	29.7	33.1	24.5	24.3	32.2	30.1
H + GA						
GA1	18.5	18.0	16.8	11.3	27.4	20.0
GA2	38.2	36.9	32.4	35.8	42.3	39.8
GA3	23.8	28.4	16.1	20.9	24.8	23.1
GA4	26.5	32.4	20.1	26.7	28.3	27.0
GA6	55.4	59.3	45.7	50.5	51.9	52.8
H + EG						
EG4	27.9	33.2	21.0	29.0	28.1	29.2
EG6	53.5	57.8	44.4	49.6	50.7	51.3

fore, we assume that the other eight reactions, including reaction type 5 and 6, can also be described with the same functional and basis set combination. As a double-check we have tested several functionals suggested by Li et al. (2016) to make sure that the activation energies obtained are of the correct magnitude, see Table A2.

APPENDIX B: RATE CONSTANTS

Tables B1– B5 give the values for the unimolecular reaction rate constants as calculated with instanton theory and corresponding to Figs 2–5 and 7 of the main manuscript.

Table B1. Unimolecular reaction rate constants [k (s^{-1})] for reaction MF + H. The instanton path was discretized using 80 images.

T (K)	MF1	MF2	MF3	MF4	MF5
75	3.60E−01	1.75E+00		1.13E−01[a]	3.77E−33
80			3.37E+00[b]	1.38E−01[b]	
85	4.80E−01	1.86E+00	4.16E+00[b]	1.61E−01[b]	1.70E−32
90	5.72E−01	1.90E+00	5.20E+00[b]	1.87E−01[b]	8.08E−32
95	6.91E−01	2.08E+00	6.47E+00[b]	2.25E−01[b]	1.78E−31
100			8.23E+00[b]	2.79E−01	
105	1.02E+00	2.54E+00	1.12E+01	3.76E−01	1.95E−30
110			1.41E+01	4.66E−01	
120			2.29E+01	7.50E−01	
130			3.77E+01	1.24E+00	
140	5.56E+00	5.60E+00	6.22E+01	2.08E+00	1.31E−26
150			1.03E+02		
160			1.70E+02		
170	2.80E+01	1.66E+01	2.78E+02	1.04E+01	2.73E−23
200	1.61E+02	5.11E+01	1.15E+03	4.93E+01	3.13E−20
250	3.80E+03	3.53E+02	9.31E+03	5.45E+02	6.43E−16
300		2.66E+03	6.22E+04	5.35E+03	1.72E−12
350		2.03E+04	3.70E+05		9.58E−10

[a] 314 images.
[b] 158 images.

Table B2. Unimolecular reaction rate constants [k (s^{-1})] for reaction GX + H. The instanton path was discretized using 80 images.

T (K)	GX1	GX2
75	9.62E+06	1.81E+03
85	1.02E+07	2.27E+03
90	1.16E+07	2.39E+03
95	1.33E+07	2.56E+03
105	1.76E+07	3.45E+03
140	6.97E+07	9.85E+03
170	2.88E+08	2.69E+04
200		7.55E+04
250		4.44E+05

Table B3. Unimolecular reaction rate constants [k (s^{-1})] for reaction GA + H. The instanton path was discretized using 80 images.

T (K)	GA1	GA2	GA3	GA4	GA6
75	2.78E+05	2.77E+02	6.83E+07	2.56E+04	9.61E−01
85	3.00E+05	1.90E+02	7.84E+07	3.23E+04	1.37E+00
90	3.22E+05	1.97E+02	8.66E+07	3.63E+04	1.36E+00
95	3.56E+05	2.24E+02	9.74E+07	4.13E+04	1.45E+00
105	4.62E+05	3.04E+02	1.26E+08	5.48E+04	1.85E+00
140	1.91E+06	1.07E+03	3.70E+08	1.57E+05	7.40E+00
170	7.83E+06	2.68E+03	9.96E+08	4.04E+05	2.77E+01
200		7.12E+03	2.72E+09	1.02E+06	9.41E+01
250		4.37E+04	1.26E+10	4.34E+06	6.25E+02
300		2.96E+05	3.96E+10	1.54E+07	4.16E+03
350					2.74E+04

Table B4. Unimolecular reaction rate constants [k (s^{-1})] for reaction EG + H. The instanton path was discretized using 80 images.

T (K)	EG4	EG6
75	3.47E+06	
85	4.60E+06	
90	5.46E+06	2.24E+03
95	6.20E+06	2.13E+03
105	7.48E+06	2.25E+03
140	2.73E+07	6.30E+03
170	7.54E+07	1.72E+04
200	2.28E+08	4.63E+04
250	1.02E+09	2.15E+05
300		1.11E+06
350		5.98E+06

Table B5. Unimolecular reaction rate constants [k (s^{-1})] for FA reactions. The instanton path was discretized using 80 images.

T (K)	FAR1	FAR2
50	1.99E+03	
55	2.29E+03	
65	3.16E+03	4.59E−09
75	4.89E+03	1.03E−08
85	7.87E+03	3.51E−08
90	9.93E+03	2.58E−07
95	1.26E+04	1.88E−07
105	2.13E+04	1.26E−06
140	1.24E+05	6.05E−04
170	5.77E+05	
200	2.63E+06	
250	2.99E+07	
300	2.62E+08	

This paper has been typeset from a TEX/LATEX file prepared by the author.